A Novel Wireless Power Transfer for In-Motion EV/PHEV Charging

Omer C. Onar, John M. Miller, Steven L. Campbell, Chester Coomer, Cliff. P. White, and Larry E. Seiber
Power Electronics and Electric Machinery Group, Energy and Transportation Science Division,
National Transportation Research Center, Oak Ridge National Laboratory
Oak Ridge, TN 37831 USA
onaroc@ornl.gov, millerjm@ornl.gov, campbellls@ornl.gov, coomercl@ornl.gov, whitecp@ornl.gov, seiberle@ornl.gov

***Abstract*—Wireless power transfer (WPT) is a convenient, safe, and autonomous means for electric and plug-in hybrid electric vehicle charging that has seen rapid growth in recent years for stationary applications. WPT does not require bulky contacts, plugs, and wires, is not affected by dirt or weather conditions, and is as efficient as conventional charging systems. When applied in-motion, WPT additionally relives range anxiety, adds further convenience, reduces battery size, and may help increase the battery life through charge sustaining approach. This study summarizes some of the recent activities of Oak Ridge National Laboratory (ORNL) in WPT charging of EV and PHEV's in-motion. Laboratory experimental results that highlight the wireless transfer of power to a moving receiver coil as it passes a pair of transmit coils and investigation of results of insertion loss due to roadway surfacing materials. Some of the experimental lessons learned are also included in this study.**

I. INTRODUCTION

WPT is emerging as a flexible, convenient, safe, and autonomous charging method for EV and PHEVs. WPT's safety stems beyond the inherent isolation between the large between the grid side transmit pad and the vehicle mounted receiver coil. Wireless charging can also be done during inclement weather without being affected from snow or rain without needing bulky cables and heavy duty plugs. The convenience and flexibility of the WPT is not only because no cables and connectors are necessary but due more to the fact that charging becomes fully autonomous [1], [2]. It is not difficult to imagine a vehicle with magnetic field sensing or a parking aide being capable of positioning itself over a primary pad for optimum alignment and autonomous charging as the technology evolves. A vehicle to infrastructure (V2I) communications can be implemented to add to the autonomy benefit by handling all the bidirectional communications needed for charging transactions as well as providing the feedback channel for power flow regulation.

Among the various previous publications reported in literature, in [3], a secondary coil design used to couple with a roadway embedded primary wire is described. The authors indicated that operating at 20 kHz and over a 10mm air gap between the primary cable at 100A and secondary coil it was possible to transfer 3 kW at 80% system efficiency. Implementing controls on both primary and secondary sides has been investigated in [4] and authors concluded that application of two controllers in both sides will increase the cost and render the system less reliable. It has also been found that the operating frequency should be adjusted as the secondary load changes. In [5], primary side regulation method is proposed based on a combination of magnitude control and energy injection concepts of the primary current. Authors of [6] focused on soft switching power inverter and pointed out with a soft ferrite backed 400 mm diameter coil with a Litz cable winding, the power could be transferred across 300 mm gap at >80% efficiency. The achievement of 90% efficiency over a 100 mm gap and application in automated guided vehicles is discussed in [7]. Additional technical content presented in [8]-[11] provide supplementary elaboration on key aspects of WPT. In [12] for example, authors note that with loosely coupling case ($0.1<k<0.5$) that the operation should be from 10 to 50 kHz. Examples of weight reduction by ferrite use minimization are provided in [10]. The findings in [10] reinforce the point that as the load changes the resonant point changes; however, the recommended operation in radiated frequency of 15.9 MHz is not of interest in WPT charging. Frequency characteristics of resonance-based wireless energy transfer are summarized in [12] and an adaptive frequency with power-level tracking system for efficient magnetic resonance is proposed in [13]. A departure from conventional coupling coil design is highlighted in [11] where the authors suggest use of multiple coils forming a WPT system. Of importance is that it is pointed out the distinction between circular and polarized pads noting that if a non-polarized circular coil equipped vehicle parks over a polarized primary pad that power will be lower, more fringing flux will be present and significant leakage results. A coupling coil solution for double-D-quadrature design that is claimed to offer a larger charge zone for misalignment is proposed by the same authors in [14] and that is compatible with non-polarized circular coils.

ORNL began investigation of wireless power transfer subsequent to the presentation in [15] describing some of the

This manuscript has been authored by UT-Battelle, LLC, under Contract DE-AC05-00OR22725 with the U.S. Department of Energy. The United States Government retains and the published, by accepting this article for publication, acknowledges that the United States Government retains a nonexclusive, paid-u, irrevocable, world-wide license to publish or reproduce the published form of this manuscript, or allows others to do so, for the Unites States Government purposes.

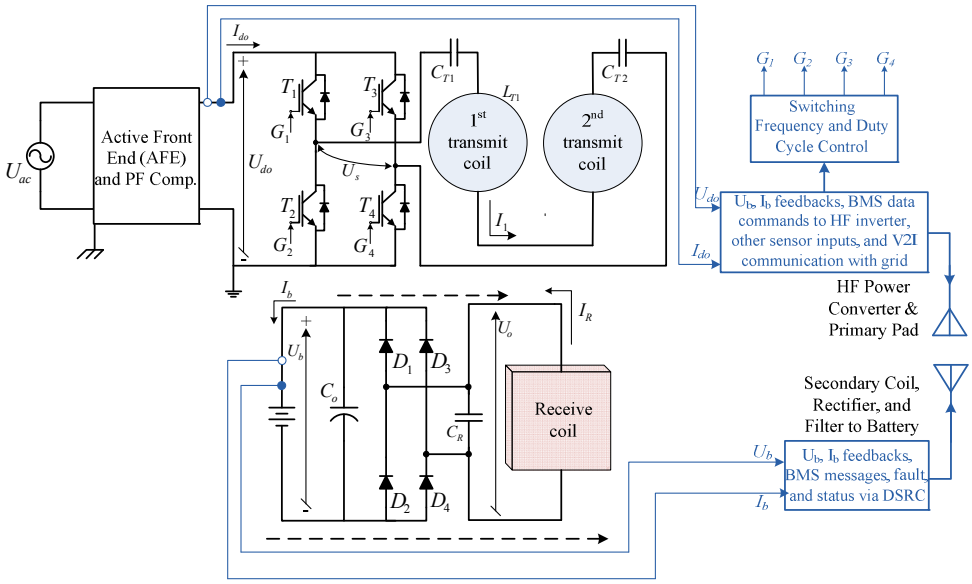

Fig. 1. In-motion wireless power transfer system layout.

work done by authors in [16]. Details of this work were then made public in 2011 [17] and advocated the use of loosely coupled magnetic resonance power transfer. With this background the ORNL team proceeded with detailed coupling coil design, fabrication and experimental validation. In this paper WPT systems developed at ORNL is augmented with a series connection of primary coils and one movable secondary coil mounted underneath a small neighborhood GEM electric vehicle to pick-up charge when the vehicle is in motion.

II. System Description

The system level diagram of ORNL's in-motion WPT system is illustrated in Fig. 1. The stationary side of the WPT system consists of a utility grid, an active front-end rectifier with power factor correction, a high frequency H-bridge inverter, and two series connected transmit coils with their series resonant tuning capacitor C_{T1} and C_{T2}. The vehicle side of the system includes a receive coil mounted underneath of the vehicle with a parallel resonant tuning capacitor C_R, a diode bridge rectifier with a DC filtering capacitor C_O, and the vehicle battery with a clamping voltage of U_b.

A. Coupling Coil Design

Coil design is of essence in WPT systems since it determines the power transfer level, overall performance and efficiency, in addition to the shielding and magnetic emissions levels to be expected. The ORNL coil design relies on Litz cable coils over a soft ferrite structure and a non-magnetic case having very low profile. Fig. 2 illustrates an adjustable fixture fabricated for a primary and secondary coil pair wound with 7 turns of 6 AWG jacketed Litz cable for the transmit coil and 5 turns on the receive coil.

In [18] the author develops the magnetic vector potential due to an ideal primary coil at a field point that lies at the location of the secondary coil. For a coil pair having a radius a, assuming infinitesimal conductor radius, and a coil to coil spacing, z. Then the radius from the primary coil origin to the field point is $r = \sqrt{(a^2 + z^2)}$ and vector potential, A_ϕ, for a case of N_1 primary turns and I_1 Amps yield a primary excitation of $N_1 I_1$ amp-turns. This primary excitation is depicted as I_{dl} in Fig. 2 where $a_1 = a_2 = a$.

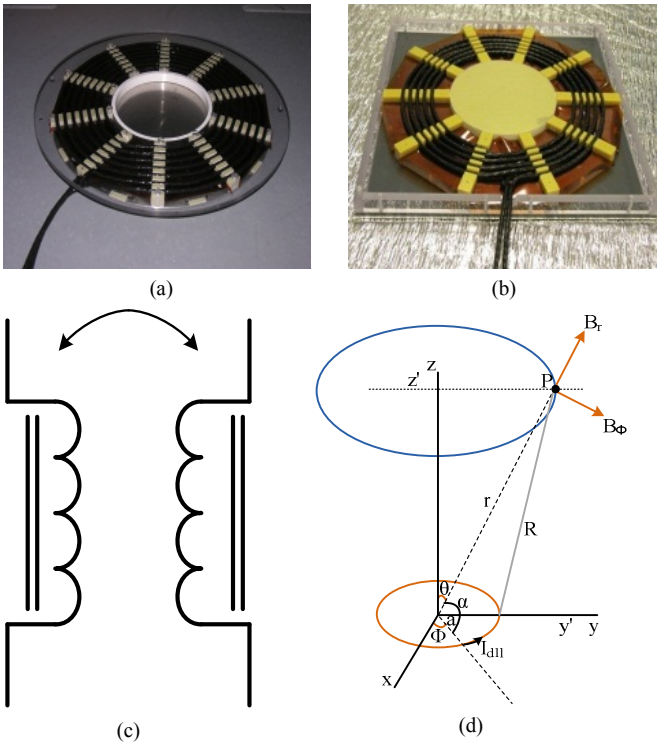

Fig. 2. Experimental fixture with distributed Litz winding: (a) 7 turns for transmit coil, (b) 5 turns for receive coil, (c) coupling coil symbol with loosely coupled transformer ferrite core back iron, and (d) vector field analysis diagram.

B. High Frequency (HF) Power Inverter Regulation

Load conditions; i.e., state-of-charge of the battery and coupling coefficient; i.e., vehicle coil to primary pad gap and any misalignment between transmit and receive coils determine the frequency response of the WPT system. The amount of power transferred to the secondary coil is governed

by the switching frequency, duty cycle, and the input voltage of the inverter. This relationship can be expressed as (1) where the HF power inverter rail voltage is U_{d0}, pulse duty ratio d, and angular frequency ω.

$$U_1(t) = \frac{4U_{d0}}{\pi}\sin\left(d\frac{\pi}{2}\right)\cos(\omega t) \quad (1)$$

Although the primary coil voltage can be controlled by the active front end converter to vary the dc rail voltage U_{d0}, the ultimate objective is to dynamically change the switching frequency and the duty cycle in order to achieve the best operating conditions in terms of efficiency and power transfer. In the ORNL laboratory setting the HF power inverter voltage was adjusted using a power supply. In a commercialized version of this WPT technology a dedicated short range communication (DSRC) link as shown in Fig.1 would be needed. The transmitter side of the DSRC collects the measurement data such as battery voltage, battery current, and battery management system (BMS) messages needed for regulation. The grid-side receiver side of the DSRC channel receives this information for control purposes along with supporting primary side measurements. Then, a DSP based embedded control system determines the switching frequency and the appropriate duty cycle according to the control law being used. The switching signals for the inverter IGBTs are generated by the DSP control algorithm and applied to the HF power inverter gate drives. The control system can also regulate the inverter power based on the reference power commands that can be received through the V2I communications from a smart grid compliant utility.

The ORNL experimental inverter shown in Fig. 3 employs dual Powerex Intellimod IGBTs in an H-bridge arrangement with each phase leg connected to one terminal of the primary coil and tuning capacitor network. The control system of the inverter is implemented within a TMS320F28335PGFA DSP module from Texas Instruments. While generating the switching signals, dead band control, shoot-through prevention, and condition monitoring based protection and termination systems have also been taken into account. For demonstration purposes, the inverter can also be controlled and monitored via RS232 by a host computer. The control system involves instantaneously varying the switching frequency and the duty ratio to adapt to the changing conditions such as battery SOC and the coupling coefficient while taking the efficiency and power transfer level into account.

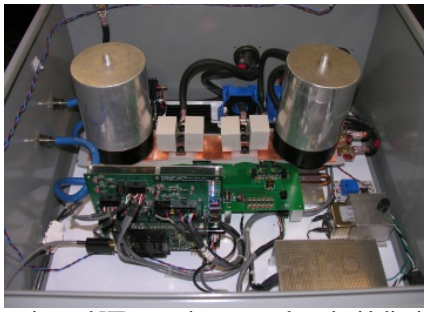

Fig. 3. Experimental HF power inverter packaged with liquid cooling.

C. System Behavior under Different Frequencies

Of particular interest for WPT is investigating the system behavior under different switching frequencies around the tuned resonant frequency. Experiments were undertaken at ORNL's WPT laboratory to assess the frequency response of the active and reactive powers at the primary and secondary coils, DC input and DC load powers, power factor, and the efficiency. During these tests, the coils are 100% aligned, gap is fixed at 100 mm, and a constant DC link voltage of 27.5 V is applied on inverter input terminals. In these tests a Chroma model 63210 battery eliminator rated 15/150A, 125/500V, 14kW is operated in constant voltage (CV) mode at the desired vehicle battery potential. For these tests a different set of coupling coils were used that had been designed for an in-motion WPT charging application of a small battery electric vehicle (a GEM electric vehicle with 72V rated battery voltage). The coils are tuned to f_{01}=23kHz with L_1=24μH, C_1=2.0μF and f_{02}=21.8kHz L_2=18.4μH, C_2=2.9μF with turns ratio, n=0.876, R_{1dc}=9.08 and R_{2dc}=11.5mΩ. When the small 330mm diameter coils are operating at z=100mm (D/z=3.3) and inverter duty d=0.8 with battery potential, U_b=80V_{dc}, the power transfer peaks at 23 kHz with a load power, P_o=2 kW.

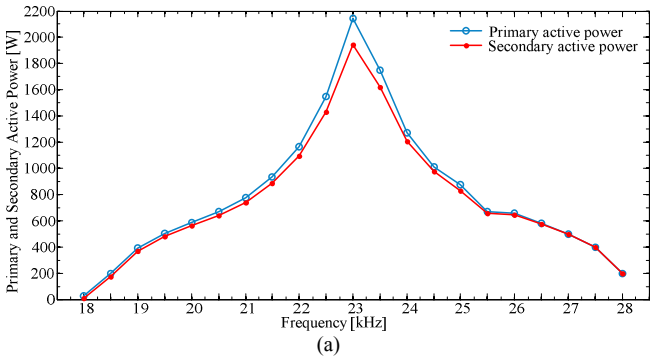

(a)

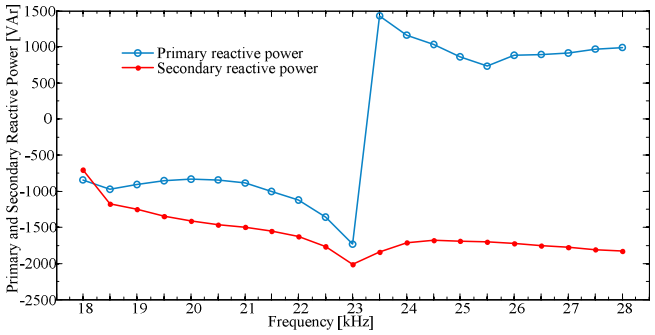

(b)

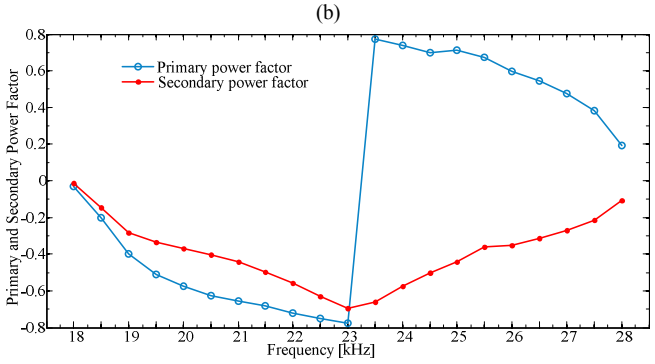

(c)

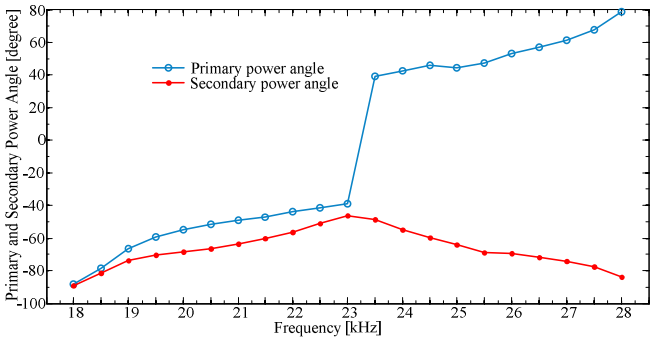

(d)

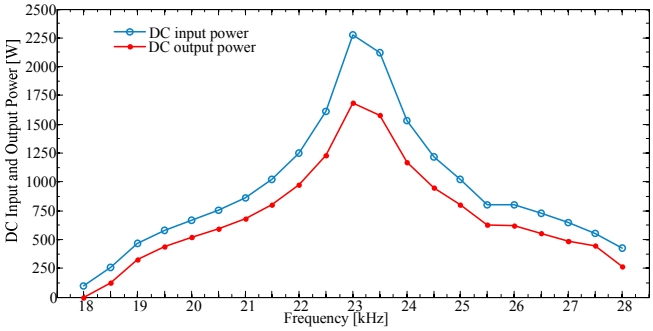

(e)

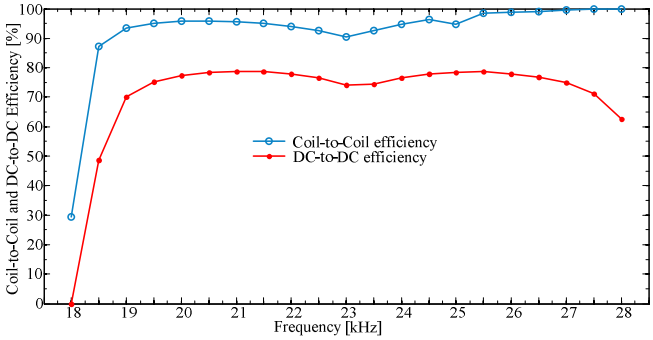

(f)

Fig. 4. Experimental results for system behavior under different frequencies: primary and secondary active power (a), primary and secondary reactive power (b), primary and secondary power factor (c), primary and secondary power angle (d), DC input and output power (e), coil-to-coil and DC-to-DC efficiency (f).

The real and reactive power variations are shown in Fig. 4 (a) and (b) whereas Fig. 4 (c) and (d) presents the primary and secondary power factor and power angle versus the frequency. Additionally, input and output DC power variations and the coil-to-coil and DC-to-DC efficiencies are demonstrated in Fig. 4 (e) and (f). As seen from Fig. 4, primary and secondary active power peaks at about 23kHz as this is the case for the DC input and output powers. When operating below the resonant frequency, the system is highly capacitive and system becomes inductive at frequencies above the resonance. At about resonant frequency, primary reactive power has a zero crossing transitioning from capacitive to inductive. In fact, this operating point should be ideally sought in order to reduce the reactive power burden on the HF power inverter.

D. Inverter Reactive Power due to U_{d0} and d

HF power inverter's reactive power burden due to the voltage control of the primary pad in the process of power flow regulation is also of particular interest.

In this specific test, the power transferred to the load is kept constant by varying the DC rail voltage and the duty cycle of the HF power inverter. According to (1), when the inverter duty ratio is varied the fundamental component of the voltage applied to the primary coil varies; however, the presence of reactive power leads to freewheeling diode conduction in the H-bridge that tends to "fill-in" the inter-pulse dead times. These circumstances can be observed in Fig. 5 (a) and (b) where frequency is 22.5kHz and *d* is 0.8 and 0.4, respectively.

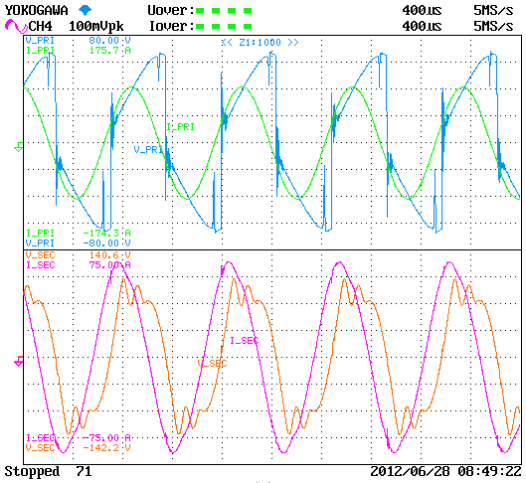

(a)

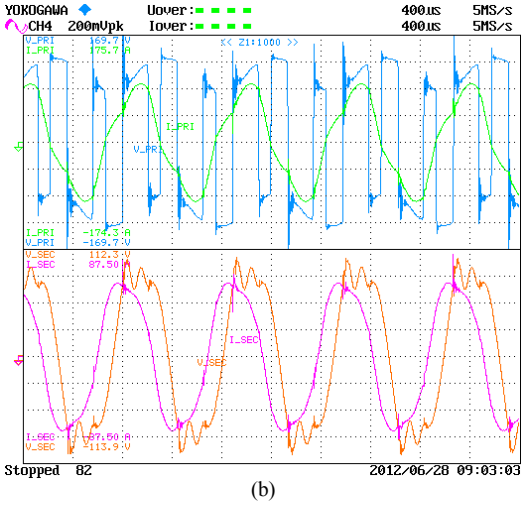

(b)

Fig. 5. Experimental results showing the effect of duty cycle being 0.8 (a) and 0.4 (b).

It can be observed that keeping the load power (i.e., power to battery eliminator) constant as duty ratio decreased required a complimentary increase in HF inverter rail voltage U_{d0}. The results are tabulated in Table I. In Table I, the heading VSI is the volt-sec-integral applied to the primary coil by the HF power inverter when the respective active switches are ON.

TABLE I
INVERTER U_{D0}-D VARIATION UNDER CONSTANT LOAD

f	***Udo***	***d***	***VSI***	***Po***	***Q_1***
[kHz]	[V_{dc}]	[#]	[mWb]	[W]	[VA]
22.5	41.87	0.8	0.743	2055	-2249
22.5	55.26	0.6	0.736	2017	-3112
22.5	117.66	0.4	1.18	2011	-7005

It should be noted that in Table I, measured reactive power Q_1 increases proportionally with the duty cycle d decreased while keeping the output power fixed. As a result, it can be stated that WPT power inverters must therefore have a much higher reactive power rating than real power rating, if a duty cycle cased control is employed.

E. Insertion Loss of Concrete and Asphalt

In future WPT system implementations, it is very likely that the primary coils will be embedded under the parking space concrete or roadway concrete or asphalt surfaces. The insertion loss contributed by the presence of common road surfacing materials in the WPT gap has been characterized for their impact on WPT loss. In Fig. 6, a sample of road surface concrete obtained from scheduled road work on US-95 near Kingston, TN is illustrated. The concrete is aged and was exposed to traffic for at least 10 years. Insertion loss of materials appears as a loss element in the WPT magnetizing branch.

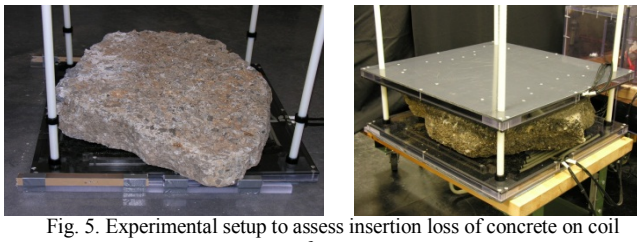

Fig. 5. Experimental setup to assess insertion loss of concrete on coil performance.

The influence of conductive materials such as flux guiding soft ferrites or aluminum shielding in the WPT active zone between primary and secondary coils is to introduce a loss term, R_c, in the magnetizing branch as shown in Fig. 6. Under open circuit conditions the magnetizing branch core loss introduces additional real power to the input that can be computed based on knowledge of the primary coil ac resistance at the test frequency. The results in Table II confirm the change in input phase angle with and without concrete present. The current source, I_1, in Fig. 6 represents the Industrial Electronics model 1500A Powertron amplifiers inject a known and clean 10.00 A_{rms} into the primary coil. The system voltages for both open and short circuit conditions are listed in Table II for reference.

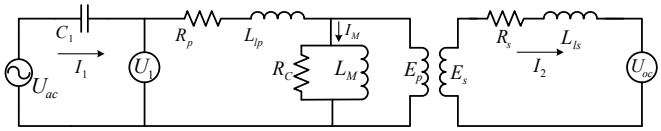

Fig. 6. WPT coil pair equivalent circuit with core insertion loss element R_c.

TABLE II
EVALUATION OF CONCRETE ON WPT PERFORMANCE

Conditions	Primary Voltage		Secondary Voltage		Phase	
	No concrete	With concrete	No concrete	With concrete	No concrete	With concrete
Open Ckt	51.95	50.76	10.78	9.3	88.89	88.42
Short Ckt	49.71	48.98	0.10	0.1	89.89	88.25

WPT core loss is calculated according to (2) under open circuit conditions (i.e., secondary unloaded) so that core loss resistance, R_c, can be separated from primary coil series resistance, R_p (primary coil resistance, R_p=38mΩ in model of Fig. 6). Under short circuit conditions an additional loss term is present due to secondary current flow in that coil yielding results also tabulated in Table II. The input current, I_1, is regulated so extraction of the coil conductor loss in R_p is readily done leaving only determination of R_c knowing the phase θ obtained from the test equipment. The primary coil input power (P_{in}) is given as (2).

$$P_{in} = \frac{U_{oc}^{\ 2}}{R_C} + I_1^{\ 2} R_p = U_1 I_1 \cos(\theta) \tag{2}$$

For the experimental coils used the core loss computed from (2) amounts to 6.26W without concrete and 13.99W with the concrete slab (110 mm thick covering the entire coil window area). The concrete therefore adds 3.93 W of additional loss under the conditions cited.

III. LABORATORY EXPERIMENTAL SETUP AND EXPERIMENTAL RESULTS

In Fig. 7, the setup of the vehicle in-motion wireless charging system built in authors' research laboratory is presented.

Fig. 7. In-motion wireless vehicle charging system setup.

As the vehicle passes through the transmit coils, measurements are taken for 9 different positions based on the location of the receiver coil underneath of the GEM vehicle. These positions are: **Position 1)** Right before alignment with the first transmit coil; edge to edge, **Position 2)** 50% aligned with the first transmit coil, **Position 3)** Perfectly aligned with the first transmit coil, **Position 4)** 50% misaligned with the first transmit coil, towards the second transmit coil, **Position 5)** Right in between two transmit coils, **Position 6)** 50% aligned with the second transmit coil, **Position 7)** : Perfectly aligned with the second transmit coil, Position 8) 50% misaligned with the second transmit coil, and **Position 9)** Right after alignment with the second transmit coil; edge to edge. These relative positions are summarized in Fig. 8. With respect to the receiver coil position, in-motion vehicle charging measurements are demonstrated in Figs. 9 to 14.

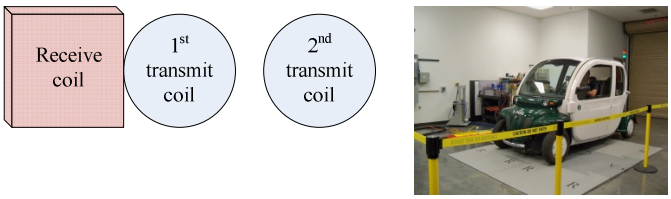

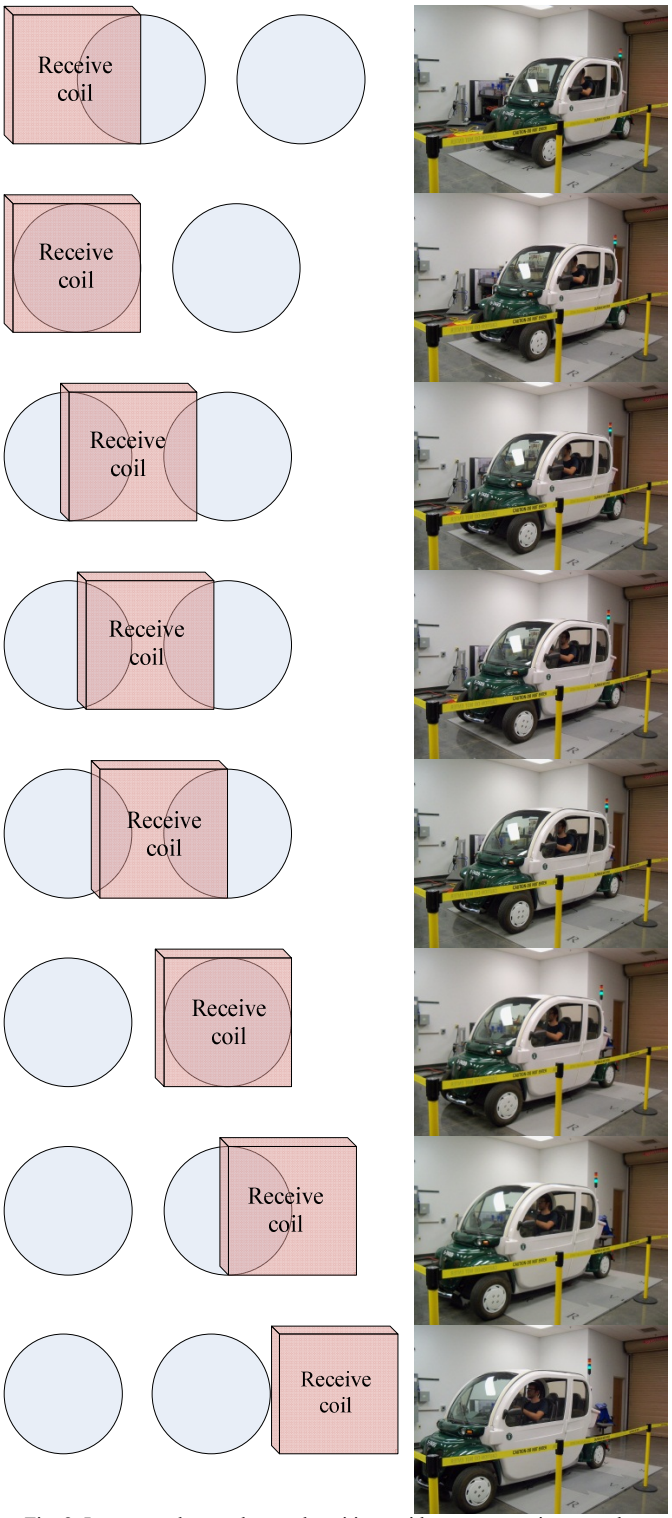

Fig. 8. Incremental secondary pad positions with respect to primary pads.

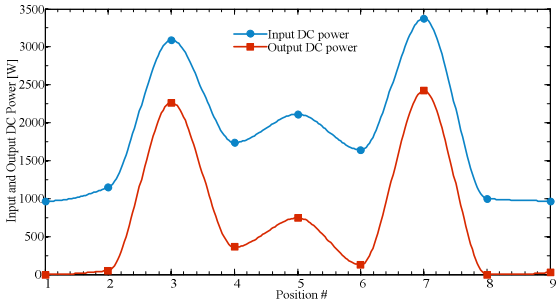

Fig. 9. Input and output power vs. position.

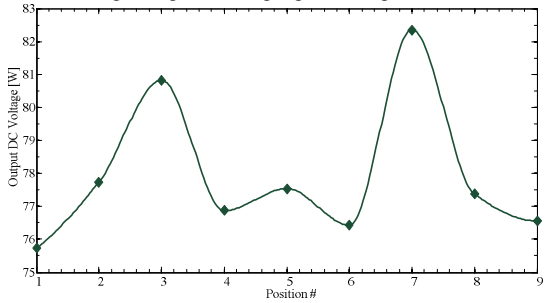

Fig. 10.Output DC voltage vs. position.

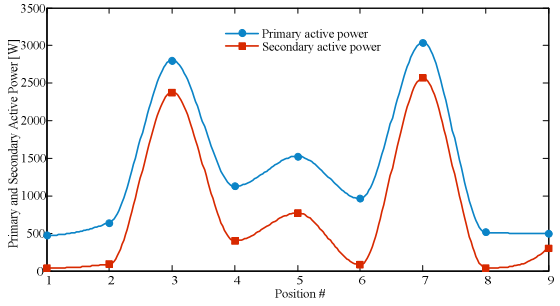

Fig. 11. Primary and secondary active power vs. position.

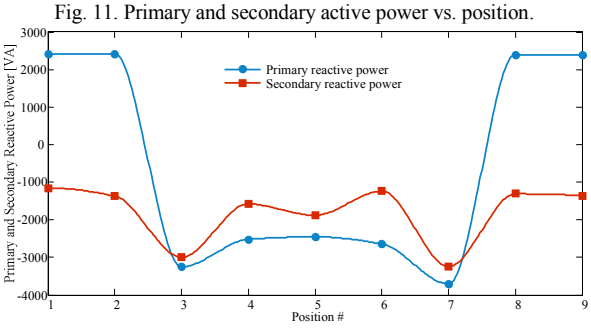

Fig. 12. Primary and secondary reactive power vs. position.

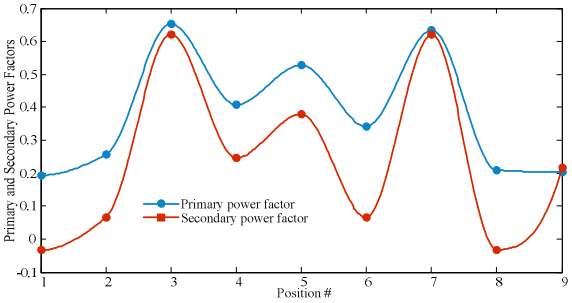

Fig. 13. Primary and secondary power factor vs. position.

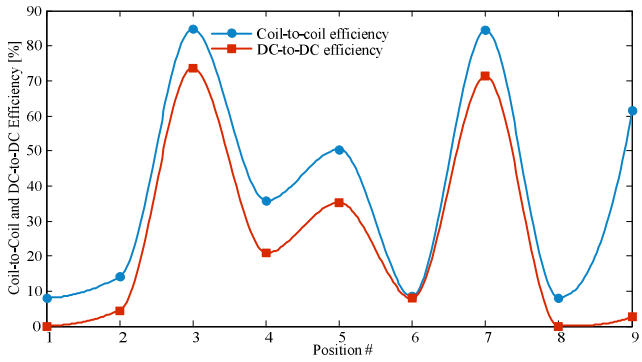

Fig. 14. Coil-to-coil and DC-to-DC efficiencies vs. position.

In addition to the power related measurements, electromagnetic field measurements have been conducted using NARDA EHP-50D field analyzer to ensure that the emitted field is within the acceptable standards for the general public level of 6.25 μT. Fig. 15 (a) and (b) show the NARDA device located at driver seat and car floor board, respectively.

(a) (b)

Fig. 15. Magnetic field measurement device locations: driver seat (a) and floor board (b).

Magnetic field measurements are summarized in Fig. 16 with respect to the measurement device locations and the secondary pad positions relative to the primary pads.

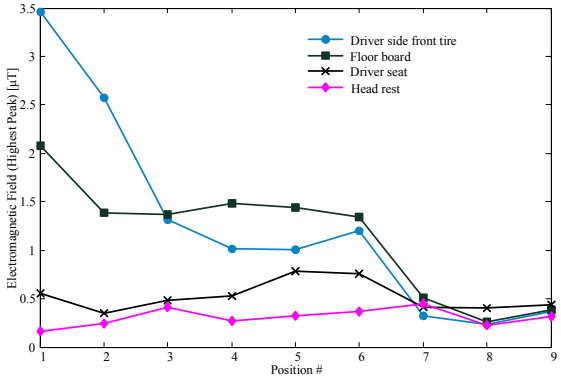

Fig. 16. Magnetic field measurement results with respect to device locations and relative coil positions.

By observing the electromagnetic field in Fig. 16 one can see all of the fields measured, with the exception of one, are well within the acceptable standards for the general public of 6.25 μT, set by the International Commission on Non-Ionizing Radiation Protection (ICRIP). The measurement at the passenger side tire was considerably higher due to the excess field was generated by the high frequency cables. The cables were extended to the side of the pad that the coils were imbedded in before connecting to the resonant capacitors. The excess field that was generated by the wires could be prevented by two different means; it would be ideal to place the capacitors right next to the coils so that no extra field is generated at all, although if there is a space constraint for the capacitors a simple thin aluminum shield can be placed over the wires to reduce the field beneath the 6.25 μT limit. By placing a 1 mm thick piece of aluminum sheet over the wires as shown in Fig. 17, the field was reduced from 18.72 μT to 3.22 μT as shown in Fig. 18. The field at the driver seat, at a maximum of 0.78 μT, is no more than that of a laptop measuring at 0.94 μT.

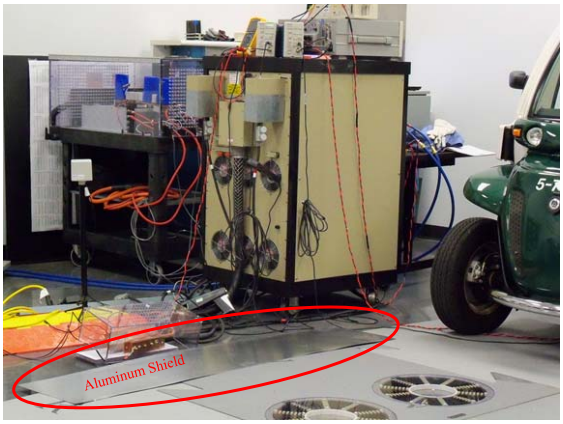

Fig. 17. Shielding with 1 mm thick piece of aluminum.

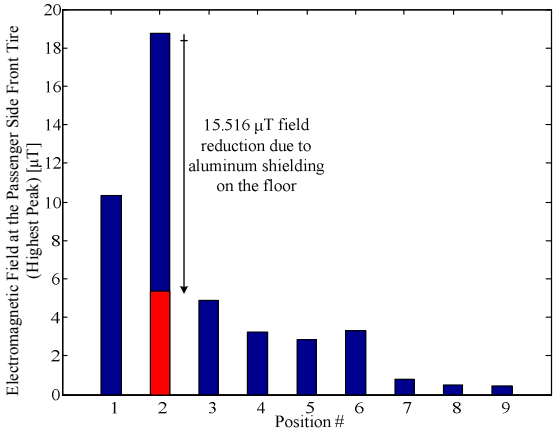

Fig. 18. Field reduction achieved with aluminum shielding.

As an example of the electromagnetic field density measurements, Fig. 19 shows the field densities in x, y, and z directions when NARDA is placed on the driver seat while the vehicle side coil is 100% aligned with the secondary coil in x-direction.

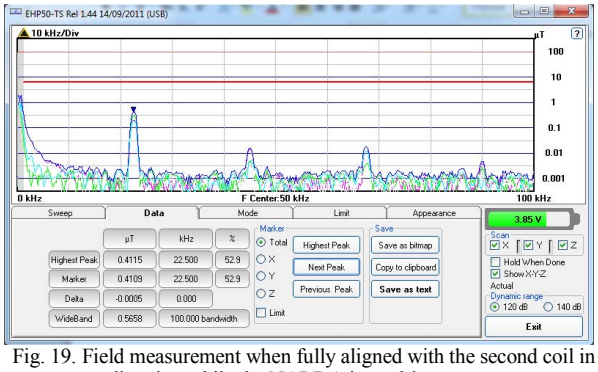

Fig. 19. Field measurement when fully aligned with the second coil in x-direction while the NARDA is on driver seat.

IV. Conclusions and Future Work

Wireless power charging of PEV's is an emerging technology that is finding widespread and rapid appeal as a safe, convenient and flexible means of charging. This paper examines the technical aspects of in-motion wireless power charging of EVs and PHEVs along with describing the proposed in-motion wireless vehicle charging topology. It is shown that a secondary (capture or receiver) coil passing across a pair (or more) of energized primary (transmit) coils results in fluctuations in the power available to recharge the vehicle battery pack. In addition to the DC input and output power, coil-to-coil and DC-to-DC efficiency and the primary and secondary active and reactive power varies with respect to the position. In addition, the effects of the highway surfacing materials such as concrete and asphalt are examined and experimental results are presented showing the effect of concrete and asphalt on the transparency of the WPT magnetic field exposure. Lastly, an overview of WPT magnetic field measurements are presented along with the effect of shielding to reduce the magnetic field below the safe limits on the passenger side front tire. In future work, a Zylinx ZP24D-250RM 2.4Ghz radio modem will be implemented for online frequency control of the system for maximized power transfer under varying conditions.

Acknowledgment

Authors would like to acknowledge. Philip M. Ryan with the Fusion Energy Division at the Oak Ridge National Laboratory for the coil finite element analyses and P. T. Jones and Paul Chambon for their assistance in vehicle systems aspects of this program at ORNL's National Transportation Research Center.

References

[1] J. M. Miller and O. C. Onar, "Oak Ridge National Laboratory in-motion wireless power transfer system," in *Proc., 1st Conference on Electric Roads and Vehicles (CERV'12)*, February 2012, Park City, UT.

[2] J. M. Miller, C. P. White, O. C. Onar, and P. M. Ryan, "Grid side regulation of wireless power charging for plug-in electric vehicles," in *Proc., IEEE Energy Conversion Congress and Exposition (ECCE'12)*, pp. 261-268, September 2012, Raleigh, NC.

[3] S. Lee, J. Huh, C. Park, N.-S. Choi, G.-H. Cho, and C.-T. Rim, "On-line electric vehicle using inductive power transfer system," in *Proc., IEEE Energy Conversion Congress and Exposition (ECCE'10)*, pp. 1598-1601, September 2010, Atlanta, GA.

[4] Y.-H. Chao, J.-J.Shieh, C.-T. Pan, W.-C. Shen, and M.-P. Chen, "A primary-side control strategy for series-parallel loosely coupled inductive power transfer systems," in *Proc., IEEE Conference on Industrial Electronics and Applications (ICIEA'07)*, pp. 2322-2327, May 2007, Harbin, China.

[5] H. L. Li, A. P. Hu, G. A. Covic, and C. Tang, "A new primary power regulation method for contactless power transfer," in *Proc., IEEE International Conference on Industrial Technology (ICIT'09)*, pp. 1-5, February 2009, Gippsland, Ausralia.

[6] R. Mecke and C. Rathge, "High frequency resonant inverter for contactless energy transmission over large air gap," in *Proc., IEEE Power Electronics Specialists Conference (PESC'04)*, pp. 1737-1743, June 2004, Aachen, Germany.

[7] Z. Pantic, S. Bhattacharya, and S. Lukic, "Optimal resonant tank design considerations for primary track compensation in inductive power transfer systems," in *Proc., IEEE Energy Conversion Congress and Exposition (ECCE'10)*, pp. 1602-1609, September 2010, Atlanta, GA.

[8] Y. Nagatsuka, N. Ehara, Y. Kaneko, S. Abe, and T. Yasuda, "Compact contactless power transfer system for electric vehicles," in *Proc., International Power Electronics Conference (IPEC'10)*, pp. 807-813, June 2010, Sapporo, Japan.

[9] F. Nakao, Y. Matsuo, M. Kitsoka, and S. Sakamoto, "Ferrite core couplers for inductive chargers," in *Proc., IEEE Power Conversion Conference (PCC'02)*, pp. 850-854, April 2002, Osaka, Japan.

[10] T. Imura, H. Okabe, and Y. Hori, "Basic experimental study on helical antennas of wireless power transfer for electric vehicles by using magnetic resonant couplings," in *Proc., IEEE Vehicle Power and Propulsion Conference(VPPC'09)*, pp. 936-940, September 2009, Dearborn, MI.

[11] G. A. Covic, M. L. G. Kissin, D. Kacprazak, N. Clausen, and H. Hao, "A bipolar primary pad topology for EV stationary charging and highway power by inductive coupling," in *Proc., IEEE Energy Conversion Congress and Exposition (ECCE'11)*, pp. 1832-1838, September 2011, Phoenix, AZ.

[12] S. Mao, R. Lu, C. Su, and C. Zhu, "Frequency characteristics of resonance-based wireless energy transfer," in *Proc., IEEE Vehicle Power and Propulsion Conference (VPPC'08)*, pp. 1-5, September 2008, Harbin, China.

[13] N. Y. Kim, K. Y. Kim, J. Choi, and C.-W. Kim, "Adaptive frequency with power-level tracking system for efficient magnetic resonance wireless power transfer," *Electronics Letters*, vol. 48, no. 8, pp. 452-454, April 2012.

[14] M. Budhia, G. A. Covic, and J. T. Boys, "Design and optimization of circular magnetic structures for lumped inductive power transfer systems," *IEEE Transactions on Power Electronics*, vol. 26, no. 11, pp. 3096-3101, November 2011.

[15] J. M. Miller, "Beyond hybrid electric vehicles," Invited presentation, *U.S. Department of Energy Engineering, Science & Technology Division (ESTD) Dual-Mode Transportation Workshop*, National Transportation Research Center (NTRC), September 2006, Knoxville, TN.

[16] C. H. Stephan, J. M. Millerm and L. C. Davis, "A program for individual sustainable mobility," *International Journal of Vehicle Autonomous Systems*, vol. 2, no. 3-4, pp. 255-277, 2004.

[17] M. B. Scudiere, J. W. McKeever, and J. M. Miller, "Design of wireless power transfer for stationary and moving hybrid electric vehicles," *SAE Worl Congress*, 2011-01-0354, April 2011, Detroit, MI.

[18] J. M. Miller, "Wireless Charging of Plug-in Electric Vehicles (PEV's)," *IEEE Power Electronics Society (PELS) Digital Media Series*, Webinar, December 2011.